

Observation of the double Dalitz decay $\eta' \rightarrow e^+e^-e^+e^-$

- M. Ablikim¹, M. N. Achasov^{11,b}, P. Adlarson⁷⁰, M. Albrecht⁴, R. Aliberti³¹, A. Amoroso^{69A,69C}, M. R. An³⁵, Q. An^{66,53}, X. H. Bai⁶¹, Y. Bai⁵², O. Bakina³², R. Baldini Ferroli^{26A}, I. Balossino^{27A}, Y. Ban^{42,g}, V. Batozskaya^{1,40}, D. Becker³¹, K. Beggsuren²⁹, N. Berger³¹, M. Bertani^{26A}, D. Bettone^{27A}, F. Bianchi^{69A,69C}, J. Bloms⁶³, A. Bortone^{69A,69C}, I. Boyko³², R. A. Briere⁵, A. Brueggemann⁶³, H. Cai⁷¹, X. Cai^{1,53}, A. Calcaterra^{26A}, G. F. Cao^{1,58}, N. Cao^{1,58}, S. A. Cetin^{57A}, J. F. Chang^{1,53}, W. L. Chang^{1,58}, G. Chelkov^{32,a}, C. Chen³⁹, Chao Chen⁵⁰, G. Chen¹, H. S. Chen^{1,58}, M. L. Chen^{1,53}, S. J. Chen³⁸, S. M. Chen⁵⁶, T. Chen¹, X. R. Chen^{28,58}, X. T. Chen¹, Y. B. Chen^{1,53}, Z. J. Chen^{23,h}, W. S. Cheng^{69C}, S. K. Choi⁵⁰, X. Chu³⁹, G. Cibinetto^{27A}, F. Cossio^{69C}, J. J. Cui⁴⁵, H. L. Dai^{1,53}, J. P. Dai⁷³, A. Dbeysi¹⁷, R. E. de Boer⁴, D. Dedovich³², Z. Y. Deng¹, A. Denig³¹, I. Denysenko³², M. Destefanis^{69A,69C}, F. De Mori^{69A,69C}, Y. Ding³⁶, J. Dong^{1,53}, L. Y. Dong^{1,58}, M. Y. Dong^{1,53,58}, X. Dong⁷¹, S. X. Du⁷⁵, P. Egorov^{32,c}, Y. L. Fan⁷¹, J. Fang^{1,53}, S. S. Fang^{1,58}, W. X. Fang¹, Y. Fang¹, R. Farinelli^{27A}, L. Fava^{69B,69C}, F. Feldbauer⁴, G. Felici^{26A}, C. Q. Feng^{66,53}, J. H. Feng⁵⁴, K Fischer⁶⁴, M. Fritsch⁴, C. Fritzsch⁶³, C. D. Fu¹, H. Gao⁵⁸, Y. N. Gao^{42,g}, Yang Gao^{66,53}, S. Garbolino^{69C}, I. Garzia^{27A,27B}, P. T. Ge⁷¹, Z. W. Ge³⁸, C. Geng⁵⁴, E. M. Gersabeck⁶², A. Gilman⁶⁴, K. Goetzen¹², L. Gong³⁶, W. X. Gong^{1,53}, W. Gradl³¹, M. Greco^{69A,69C}, L. M. Gu³⁸, M. H. Gu^{1,53}, Y. T. Gu¹⁴, C. Y. Guan^{1,58}, A. Q. Guo^{28,58}, L. B. Guo³⁷, R. P. Guo⁴⁴, Y. P. Guo^{10,f}, A. Guskov^{32,a}, T. T. Han⁴⁵, W. Y. Han³⁵, X. Q. Hao¹⁸, F. A. Harris⁶⁰, K. K. He⁵⁰, K. L. He^{1,58}, F. H. Heinsius⁴, C. H. Heinz³¹, Y. K. Heng^{1,53,58}, C. Herold⁵⁵, M. Himmelreich^{31,d}, G. Y. Hou^{1,58}, Y. R. Hou⁵⁸, Z. L. Hou¹, H. M. Hu^{1,58}, J. F. Hu^{51,i}, T. Hu^{1,53,58}, Y. Hu¹, G. S. Huang^{66,53}, K. X. Huang⁵⁴, L. Q. Huang^{28,58}, X. T. Huang⁴⁵, Y. P. Huang¹, Z. Huang^{42,g}, T. Hussain⁶⁸, N. Hüskens^{25,31}, W. Imoehl²⁵, M. Irshad^{66,53}, J. Jackson²⁵, S. Jaeger⁴, S. Janchiy²⁹, E. Jang⁵⁰, J. H. Jeong⁵⁰, Q. Ji¹, Q. P. Ji¹⁸, X. B. Ji^{1,58}, X. L. Ji^{1,53}, Y. Y. Ji⁴⁵, Z. K. Jia^{66,53}, H. B. Jiang⁴⁵, S. S. Jiang³⁵, X. S. Jiang^{1,53,58}, Y. Jiang⁵⁸, J. B. Jiao⁴⁵, Z. Jiao²¹, S. Jin³⁸, Y. Jin⁶¹, M. Q. Jing^{1,58}, T. Johansson⁷⁰, N. Kalantar-Nayestanaki⁵⁹, X. S. Kang³⁶, R. Kappert⁵⁹, M. Kavatsyuk⁵⁹, B. C. Ke⁷⁵, I. K. Keshk⁴, A. Khoukaz⁶³, R. Kiuchi¹, R. Kliemt¹², L. Koch³³, O. B. Kolcu^{57A}, B. Kopf⁴, M. Kuemmel⁴, M. Kuessner⁴, A. Kupsc^{40,70}, W. Kühn³³, J. J. Lane⁶², J. S. Lange³³, P. Larin¹⁷, A. Lavania²⁴, L. Lavezzi^{69A,69C}, Z. H. Lei^{66,53}, H. Leithoff³¹, M. Lellmann³¹, T. Lenz³¹, C. Li⁴³, C. Li³⁹, C. H. Li³⁵, Cheng Li^{66,53}, D. M. Li⁷⁵, F. Li^{1,53}, G. Li¹, H. Li^{66,53}, H. Li⁴⁷, H. B. Li^{1,58}, H. J. Li¹⁸, H. N. Li^{51,i}, J. Q. Li⁴, J. S. Li⁵⁴, J. W. Li⁴⁵, Ke Li¹, L. J Li¹, L. K. Li¹, Lei Li³, M. H. Li³⁹, P. R. Li^{34,j,k}, S. X. Li¹⁰, S. Y. Li⁵⁶, T. Li⁴⁵, W. D. Li^{1,58}, W. G. Li¹, X. H. Li^{66,53}, X. L. Li⁴⁵, Xiaoyu Li^{1,58}, Y. G. Li^{42,g}, Z. X. Li¹⁴, H. Liang³⁰, H. Liang^{1,58}, H. Liang^{66,53}, Y. F. Liang⁴⁹, Y. T. Liang^{28,58}, G. R. Liao¹³, L. Z. Liao⁴⁵, J. Libby²⁴, A. Limphirat⁵⁵, C. X. Lin⁵⁴, D. X. Lin^{28,58}, T. Lin¹, B. J. Liu¹, C. X. Liu¹, D. Liu^{17,66}, F. H. Liu⁴⁸, Fang Liu¹, Feng Liu⁶, G. M. Liu^{51,i}, H. Liu^{34,j,k}, H. B. Liu¹⁴, H. M. Liu^{1,58}, Huanhuan Liu¹, Huihui Liu¹⁹, J. B. Liu^{66,53}, J. L. Liu⁶⁷, J. Y. Liu^{1,58}, K. Liu¹, K. Y. Liu³⁶, Ke Liu²⁰, L. Liu^{66,53}, Lu Liu³⁹, M. H. Liu^{10,f}, P. L. Liu¹, Q. Liu⁵⁸, S. B. Liu^{66,53}, T. Liu^{10,f}, W. K. Liu³⁹, W. M. Liu^{66,53}, X. Liu^{34,j,k}, Y. Liu^{34,j,k}, Y. B. Liu³⁹, Z. A. Liu^{1,53,58}, Z. Q. Liu⁴⁵, X. C. Lou^{1,53,58}, F. X. Lu⁵⁴, H. J. Lu²¹, J. G. Lu^{1,53}, X. L. Lu¹, Y. Lu⁷, Y. P. Lu^{1,53}, Z. H. Lu¹, C. L. Luo³⁷, M. X. Luo⁷⁴, T. Luo^{10,f}, X. L. Luo^{1,53}, X. R. Lyu⁵⁸, Y. F. Lyu³⁹, F. C. Ma³⁶, H. L. Ma¹, L. L. Ma⁴⁵, M. M. Ma^{1,58}, Q. M. Ma¹, R. Q. Ma^{1,58}, R. T. Ma⁵⁸, X. Y. Ma^{1,53}, Y. Ma^{42,g}, F. E. Maas¹⁷, M. Maggiore^{69A,69C}, S. Maldaner⁴, S. Malde⁶⁴, Q. A. Malik⁶⁸, A. Mangoni^{26B}, Y. J. Mao^{42,g}, Z. P. Mao¹, S. Marcello^{69A,69C}, Z. X. Meng⁶¹, G. Mezzadri^{27A}, H. Miao¹, T. J. Min³⁸, R. E. Mitchell²⁵, X. H. Mo^{1,53,58}, N. Yu. Muchnoi^{11,b}, Y. Nefedov³², F. Nerling^{17,d}, I. B. Nikolaev^{11,b}, Z. Ning^{1,53}, S. Nisar^{9,l}, Y. Niu⁴⁵, S. L. Olsen⁵⁸, Q. Ouyang^{1,53,58}, S. Pacetti^{26B,26C}, X. Pan^{10,f}, Y. Pan⁵², A. Pathak³⁰, M. Pelizaeus⁴, H. P. Peng^{66,53}, K. Peters^{12,d}, J. L. Ping³⁷, R. G. Ping^{1,58}, S. Plura³¹, S. Pogodin³², V. Prasad^{66,53}, F. Z. Qi¹, H. Qi^{66,53}, H. R. Qi⁵⁶, M. Qi³⁸, T. Y. Qi^{10,f}, S. Qian^{1,53}, W. B. Qian⁵⁸, Z. Qian⁵⁴, C. F. Qiao⁵⁸, J. J. Qin⁶⁷, L. Q. Qin¹³, X. P. Qin^{10,f}, X. S. Qin⁴⁵, Z. H. Qin^{1,53}, J. F. Qiu¹, S. Q. Qu³⁹, S. Q. Qu⁵⁶, K. H. Rashid⁶⁸, C. F. Redmer³¹, K. J. Ren³⁵, A. Rivetti^{69C}, V. Rodin⁵⁹, M. Rolo^{69C}, G. Rong^{1,58}, Ch. Rosner¹⁷, S. N. Ruan³⁹, H. S. Sang⁶⁶, A. Sarantsev^{32,c}, Y. Schelhaas³¹, C. Schnier⁴, K. Schoenning⁷⁰, M. Scodeggio^{27A,27B}, K. Y. Shan^{10,f}, W. Shan²², X. Y. Shan^{66,53}, J. F. Shangguan⁵⁰, L. G. Shao^{1,58}, M. Shao^{66,53}, C. P. Shen^{10,f}, H. F. Shen^{1,58}, X. Y. Shen^{1,58}, B. A. Shi⁵⁸, H. C. Shi^{66,53}, J. Y. Shi¹, q. q. Shi⁵⁰, R. S. Shi^{1,58}, X. Shi^{1,53}, X. D. Shi^{66,53}, J. J. Song¹⁸, W. M. Song^{30,1}, Y. X. Song^{42,g}, S. Sosio^{69A,69C}, S. Spataro^{69A,69C}, F. Stieler³¹, K. X. Su⁷¹, P. P. Su⁵⁰, Y. J. Su⁵⁸, G. X. Sun¹, H. Sun⁵⁸, H. K. Sun¹, J. F. Sun¹⁸, L. Sun⁷¹, S. S. Sun^{1,58}, T. Sun^{1,58}, W. Y. Sun³⁰, X Sun^{23,h}, Y. J. Sun^{66,53}, Y. Z. Sun¹, Z. T. Sun⁴⁵, Y. H. Tan⁷¹, Y. X. Tan^{66,53}, C. J. Tang⁴⁹, G. Y. Tang¹, J. Tang⁵⁴, L. Y. Tao⁶⁷, Q. T. Tao^{23,h}, M. Tat⁶⁴, J. X. Teng^{66,53}, V. Thoren⁷⁰, W. H. Tian⁴⁷, Y. Tian^{28,58}, I. Uman^{57B}, B. Wang¹, B. L. Wang⁵⁸, C. W. Wang³⁸, D. Y. Wang^{42,g}, F. Wang⁶⁷, H. J. Wang^{34,j,k}, H. P. Wang^{1,58}, K. Wang^{1,53}, L. L. Wang¹, M. Wang⁴⁵, M. Z. Wang^{42,g}, Meng Wang^{1,58}, S. Wang¹³, S. Wang^{10,f}, T. Wang^{10,f}, T. J. Wang³⁹, W. Wang⁵⁴, W. H. Wang⁷¹, W. P. Wang^{66,53}, X. Wang^{42,g}, X. F. Wang^{34,j,k}, X. L. Wang^{10,f}, Y. Wang⁵⁶, Y. D. Wang⁴¹, Y. F. Wang^{1,53,58}, Y. H. Wang⁴³, Y. Q. Wang¹, Yaqian Wang^{16,1}, Z. Wang^{1,53}, Z. Y. Wang^{1,58}, Ziyi Wang⁵⁸, D. H. Wei¹³, F. Weidner⁶³, S. P. Wen¹, D. J. White⁶², U. Wiedner⁴, G. Wilkinson⁶⁴, M. Wolke⁷⁰, L. Wollenberg⁴, J. F. Wu^{1,58}, L. H. Wu¹, L. J. Wu^{1,58}, X. Wu^{10,f}, X. H. Wu³⁰, Y. Wu⁶⁶, Y. J. Wu²⁸, Z. Wu^{1,53}, L. Xia^{66,53}, T. Xiang^{42,g}, D. Xiao^{34,j,k}, G. Y. Xiao³⁸, H. Xiao^{10,f}, S. Y. Xiao¹, Y. L. Xiao^{10,f}, Z. J. Xiao³⁷, C. Xie³⁸, X. H. Xie^{42,g}, Y. Xie⁴⁵, Y. G. Xie^{1,53}, Y. H. Xie⁶, Z. P. Xie^{66,53}, T. Y. Xing^{1,58}, C. F. Xu¹, C. J. Xu⁵⁴, G. F. Xu¹, H. Y. Xu⁶¹, Q. J. Xu¹⁵, X. P. Xu⁵⁰, Y. C. Xu⁵⁸, Z. P. Xu³⁸, F. Yan^{10,f}, L. Yan^{10,f}, W. B. Yan^{66,53}, W. C. Yan⁷⁵, H. J. Yang^{46,e}, H. L. Yang³⁰, H. X. Yang¹, L. Yang⁴⁷, S. L. Yang⁵⁸, Tao Yang¹, Y. F. Yang³⁹, Y. X. Yang^{1,58}, Yifan Yang^{1,58}, M. Ye^{1,53}, M. H. Ye⁸, J. H. Yin¹, Z. Y. You⁵⁴, B. X. Yu^{1,53,58}, C. X. Yu³⁹, G. Yu^{1,58}, T. Yu⁶⁷, X. D. Yu^{42,g}, C. Z. Yuan^{1,58}, L. Yuan², S. C. Yuan¹, X. Q. Yuan¹, Y. Yuan^{1,58}, Z. Y. Yuan⁵⁴, C. X. Yue³⁵, A. A. Zafar⁶⁸, F. R. Zeng⁴⁵, X. Zeng⁶, Y. Zeng^{23,h}, Y. H. Zhan⁵⁴, A. Q. Zhang¹, B. L. Zhang¹, B. X. Zhang¹, D. H. Zhang³⁹, G. Y. Zhang¹⁸, H. Zhang⁶⁶, H. H. Zhang⁵⁴, H. H. Zhang³⁰, H. Y. Zhang^{1,53}, J. L. Zhang⁷², J. Q. Zhang³⁷, J. W. Zhang^{1,53,58}, J. X. Zhang^{34,j,k}, J. Y. Zhang¹, J. Z. Zhang^{1,58}, Jianyu Zhang^{1,58}, Jiawei Zhang^{1,58}, L. M. Zhang⁵⁶, L. Q. Zhang⁵⁴, Lei Zhang³⁸, P. Zhang¹, Q. Y. Zhang^{35,75}, Shuihan Zhang^{1,58}, Shulei Zhang^{23,h},

X. D. Zhang⁴¹, X. M. Zhang¹, X. Y. Zhang⁵⁰, X. Y. Zhang⁴⁵, Y. Zhang⁶⁴, Y. T. Zhang⁷⁵, Y. H. Zhang^{1,53}, Yan Zhang^{66,53}, Yao Zhang¹, Z. H. Zhang¹, Z. Y. Zhang⁷¹, Z. Y. Zhang³⁹, G. Zhao¹, J. Zhao³⁵, J. Y. Zhao^{1,58}, J. Z. Zhao^{1,53}, Lei Zhao^{66,53}, Ling Zhao¹, M. G. Zhao³⁹, Q. Zhao¹, S. J. Zhao⁷⁵, Y. B. Zhao^{1,53}, Y. X. Zhao^{28,58}, Z. G. Zhao^{66,53}, A. Zhemchugov^{32,a}, B. Zheng⁶⁷, J. P. Zheng^{1,53}, Y. H. Zheng⁵⁸, B. Zhong³⁷, C. Zhong⁶⁷, X. Zhong⁵⁴, H. Zhou⁴⁵, L. P. Zhou^{1,58}, X. Zhou⁷¹, X. K. Zhou⁵⁸, X. R. Zhou^{66,53}, X. Y. Zhou³⁵, Y. Z. Zhou^{10,f}, J. Zhu³⁹, K. Zhu¹, K. J. Zhu^{1,53,58}, L. X. Zhu⁵⁸, S. H. Zhu⁶⁵, S. Q. Zhu³⁸, T. J. Zhu⁷², W. J. Zhu^{10,f}, Y. C. Zhu^{66,53}, Z. A. Zhu^{1,58}, B. S. Zou¹, J. H. Zou¹

(BESIII Collaboration)

¹ Institute of High Energy Physics, Beijing 100049, People's Republic of China

² Beihang University, Beijing 100191, People's Republic of China

³ Beijing Institute of Petrochemical Technology, Beijing 102617, People's Republic of China

⁴ Bochum Ruhr-University, D-44780 Bochum, Germany

⁵ Carnegie Mellon University, Pittsburgh, Pennsylvania 15213, USA

⁶ Central China Normal University, Wuhan 430079, People's Republic of China

⁷ Central South University, Changsha 410083, People's Republic of China

⁸ China Center of Advanced Science and Technology, Beijing 100190, People's Republic of China

⁹ COMSATS University Islamabad, Lahore Campus, Defence Road, Off Raiwind Road, 54000 Lahore, Pakistan

¹⁰ Fudan University, Shanghai 200433, People's Republic of China

¹¹ G.I. Budker Institute of Nuclear Physics SB RAS (BINP), Novosibirsk 630090, Russia

¹² GSI Helmholtzcentre for Heavy Ion Research GmbH, D-64291 Darmstadt, Germany

¹³ Guangxi Normal University, Guilin 541004, People's Republic of China

¹⁴ Guangxi University, Nanning 530004, People's Republic of China

¹⁵ Hangzhou Normal University, Hangzhou 310036, People's Republic of China

¹⁶ Hebei University, Baoding 071002, People's Republic of China

¹⁷ Helmholtz Institute Mainz, Staudinger Weg 18, D-55099 Mainz, Germany

¹⁸ Henan Normal University, Xinxiang 453007, People's Republic of China

¹⁹ Henan University of Science and Technology, Luoyang 471003, People's Republic of China

²⁰ Henan University of Technology, Zhengzhou 450001, People's Republic of China

²¹ Huangshan College, Huangshan 245000, People's Republic of China

²² Hunan Normal University, Changsha 410081, People's Republic of China

²³ Hunan University, Changsha 410082, People's Republic of China

²⁴ Indian Institute of Technology Madras, Chennai 600036, India

²⁵ Indiana University, Bloomington, Indiana 47405, USA

²⁶ INFN Laboratori Nazionali di Frascati, (A)INFN Laboratori Nazionali di Frascati, I-00044, Frascati, Italy; (B)INFN Sezione di Perugia, I-06100, Perugia, Italy; (C)University of Perugia, I-06100, Perugia, Italy

²⁷ INFN Sezione di Ferrara, (A)INFN Sezione di Ferrara, I-44122, Ferrara, Italy; (B)University of Ferrara, I-44122, Ferrara, Italy

²⁸ Institute of Modern Physics, Lanzhou 730000, People's Republic of China

²⁹ Institute of Physics and Technology, Peace Avenue 54B, Ulaanbaatar 13330, Mongolia

³⁰ Jilin University, Changchun 130012, People's Republic of China

³¹ Johannes Gutenberg University of Mainz, Johann-Joachim-Becher-Weg 45, D-55099 Mainz, Germany

³² Joint Institute for Nuclear Research, 141980 Dubna, Moscow region, Russia

³³ Justus-Liebig-Universitaet Giessen, II. Physikalisches Institut, Heinrich-Buff-Ring 16, D-35392 Giessen, Germany

³⁴ Lanzhou University, Lanzhou 730000, People's Republic of China

³⁵ Liaoning Normal University, Dalian 116029, People's Republic of China

³⁶ Liaoning University, Shenyang 110036, People's Republic of China

³⁷ Nanjing Normal University, Nanjing 210023, People's Republic of China

³⁸ Nanjing University, Nanjing 210093, People's Republic of China

³⁹ Nankai University, Tianjin 300071, People's Republic of China

⁴⁰ National Centre for Nuclear Research, Warsaw 02-093, Poland

⁴¹ North China Electric Power University, Beijing 102206, People's Republic of China

⁴² Peking University, Beijing 100871, People's Republic of China

⁴³ Qufu Normal University, Qufu 273165, People's Republic of China

⁴⁴ Shandong Normal University, Jinan 250014, People's Republic of China

⁴⁵ Shandong University, Jinan 250100, People's Republic of China

⁴⁶ Shanghai Jiao Tong University, Shanghai 200240, People's Republic of China

⁴⁷ Shanxi Normal University, Linfen 041004, People's Republic of China

⁴⁸ Shanxi University, Taiyuan 030006, People's Republic of China

⁴⁹ Sichuan University, Chengdu 610064, People's Republic of China

⁵⁰ Soochow University, Suzhou 215006, People's Republic of China

⁵¹ South China Normal University, Guangzhou 510006, People's Republic of China

⁵² Southeast University, Nanjing 211100, People's Republic of China

⁵³ State Key Laboratory of Particle Detection and Electronics, Beijing 100049, Hefei 230026, People's Republic of China

- ⁵⁴ Sun Yat-Sen University, Guangzhou 510275, People's Republic of China
⁵⁵ Suranaree University of Technology, University Avenue 111, Nakhon Ratchasima 30000, Thailand
⁵⁶ Tsinghua University, Beijing 100084, People's Republic of China
⁵⁷ Turkish Accelerator Center Particle Factory Group, (A)Istinye University, 34010, Istanbul, Turkey; (B)Near East University, Nicosia, North Cyprus, Mersin 10, Turkey
⁵⁸ University of Chinese Academy of Sciences, Beijing 100049, People's Republic of China
⁵⁹ University of Groningen, NL-9747 AA Groningen, The Netherlands
⁶⁰ University of Hawaii, Honolulu, Hawaii 96822, USA
⁶¹ University of Jinan, Jinan 250022, People's Republic of China
⁶² University of Manchester, Oxford Road, Manchester, M13 9PL, United Kingdom
⁶³ University of Muenster, Wilhelm-Klemm-Strasse 9, 48149 Muenster, Germany
⁶⁴ University of Oxford, Keble Road, Oxford OX13RH, United Kingdom
⁶⁵ University of Science and Technology Liaoning, Anshan 114051, People's Republic of China
⁶⁶ University of Science and Technology of China, Hefei 230026, People's Republic of China
⁶⁷ University of South China, Hengyang 421001, People's Republic of China
⁶⁸ University of the Punjab, Lahore-54590, Pakistan
⁶⁹ University of Turin and INFN, (A)University of Turin, I-10125, Turin, Italy; (B)University of Eastern Piedmont, I-15121, Alessandria, Italy; (C)INFN, I-10125, Turin, Italy
⁷⁰ Uppsala University, Box 516, SE-75120 Uppsala, Sweden
⁷¹ Wuhan University, Wuhan 430072, People's Republic of China
⁷² Xinyang Normal University, Xinyang 464000, People's Republic of China
⁷³ Yunnan University, Kunming 650500, People's Republic of China
⁷⁴ Zhejiang University, Hangzhou 310027, People's Republic of China
⁷⁵ Zhengzhou University, Zhengzhou 450001, People's Republic of China
- ^a Also at the Moscow Institute of Physics and Technology, Moscow 141700, Russia
^b Also at the Novosibirsk State University, Novosibirsk, 630090, Russia
^c Also at the NRC "Kurchatov Institute", PNPI, 188300, Gatchina, Russia
^d Also at Goethe University Frankfurt, 60323 Frankfurt am Main, Germany
^e Also at Key Laboratory for Particle Physics, Astrophysics and Cosmology, Ministry of Education; Shanghai Key Laboratory for Particle Physics and Cosmology; Institute of Nuclear and Particle Physics, Shanghai 200240, People's Republic of China
^f Also at Key Laboratory of Nuclear Physics and Ion-beam Application (MOE) and Institute of Modern Physics, Fudan University, Shanghai 200443, People's Republic of China
^g Also at State Key Laboratory of Nuclear Physics and Technology, Peking University, Beijing 100871, People's Republic of China
^h Also at School of Physics and Electronics, Hunan University, Changsha 410082, China
ⁱ Also at Guangdong Provincial Key Laboratory of Nuclear Science, Institute of Quantum Matter, South China Normal University, Guangzhou 510006, China
^j Also at Frontiers Science Center for Rare Isotopes, Lanzhou University, Lanzhou 730000, People's Republic of China
^k Also at Lanzhou Center for Theoretical Physics, Lanzhou University, Lanzhou 730000, People's Republic of China
^l Also at the Department of Mathematical Sciences, IBA, Karachi, Pakistan

Based on $(10087 \pm 44) \times 10^6$ J/ψ events collected with the BESIII detector at BEPCII, the double Dalitz decay $\eta' \rightarrow e^+e^-e^+e^-$ is observed for the first time via the $J/\psi \rightarrow \gamma\eta'$ decay process. The significance is found to be 5.7σ with systematic uncertainties taken into consideration. Its branching fraction is determined to be $\mathcal{B}(\eta' \rightarrow e^+e^-e^+e^-) = (4.5 \pm 1.0(\text{stat.}) \pm 0.5(\text{sys.})) \times 10^{-6}$.

I. INTRODUCTION

The double Dalitz decays $\mathcal{P} \rightarrow \ell^+\ell^-\ell'^+\ell'^-$, where \mathcal{P} is a pseudoscalar meson ($\mathcal{P} = \pi^0, \eta$, or η') while ℓ and ℓ' are leptons ($\ell, \ell' = e, \mu$), are expected to proceed through an intermediate state of two virtual photons. These processes are of great interest for understanding the pseudoscalar transition form factor (TFF) and the interactions between pseudoscalars and virtual photons [1, 2]. These TFFs are necessary inputs to calculate the pseudoscalar-meson-pole contributions to the hadronic light-by-light scattering, which causes the second largest uncertainty in the Standard Model determi-

nation of the muon anomalous magnetic moment [3–6]. Particularly, the double Dalitz decays of pseudoscalar mesons help to determine the TFFs in the small time-like momentum region, i.e. $m_{ll}^2 \leq q^2 \leq m_P^2$, with m_{ll} the invariant mass of the dilepton and m_P the mass of the pseudoscalar meson, and thus are suitable to determine the slope of the TFFs at $q^2 = 0$ [3].

The pseudoscalar meson double Dalitz decays have been elucidated by many physics models, such as the hidden gauge model [2], the modified vector meson dominance model [2], the data driven approach [1], and the resonance chiral symmetric approach [7]. Experimental searches have been carried out in a variety of processes.

The π^0 Dalitz decay $\pi^0 \rightarrow e^+e^-e^+e^-$ has been intensively studied, and its branching fraction (BF) is determined to be $(3.38 \pm 0.16) \times 10^{-5}$ [8], which is dominated by a measurement from the KTeV Collaboration [9]. The KLOE Collaboration reported the first observation of $\eta \rightarrow e^+e^-e^+e^-$ with a BF of $(2.4 \pm 0.2(\text{stat.}) \pm 0.1(\text{sys.})) \times 10^{-5}$ [10]. The WASA Collaboration set the upper limits at the 90% confidence level of $\mathcal{B}(\eta \rightarrow e^+e^-\mu^+\mu^-) < 1.6 \times 10^{-4}$ and $\mathcal{B}(\eta \rightarrow \mu^+\mu^-\mu^+\mu^-) < 3.6 \times 10^{-4}$ [11]. However, the double Dalitz decay of η' has not been observed to date.

The theoretical predictions for $\eta' \rightarrow e^+e^-e^+e^-$ BF are in the range of $(2.1 - 2.4) \times 10^{-6}$ [1, 2], which makes it possible to be observed based on $(10087 \pm 44) \times 10^6$ J/ψ events collected in the years of 2009, 2012, 2018, and 2019 at BESIII [12] through the $J/\psi \rightarrow \gamma\eta'$ process.

II. BESIII DETECTOR AND MONTE CARLO SIMULATION

The BESIII detector [13] records symmetric e^+e^- collisions provided by the BEPCII storage ring [14], which operates in the center-of-mass energy range between 2.0 and 4.95 GeV. BESIII has collected large data samples in this energy region [15]. The cylindrical core of the BESIII detector covers 93% of the full solid angle and consists of a helium-based multilayer drift chamber (MDC), a plastic scintillator time-of-flight system (TOF), and a CsI(Tl) electromagnetic calorimeter (EMC), which are all enclosed in a superconducting solenoidal magnet providing a 1.0 T (0.9 T in 2012) magnetic field. The solenoid is supported by an octagonal flux-return yoke with resistive plate counter muon identification modules interleaved with steel. The charged-particle momentum resolution at $1 \text{ GeV}/c$ is 0.5%, and the dE/dx resolution is 6% for electrons from Bhabha scattering. The EMC measures photon energies with a resolution of 2.5% (5%) at 1 GeV in the barrel (end cap) region. The time resolution in the TOF barrel region is 68 ps, while that in the end cap region was initially 110 ps. The end cap TOF system was upgraded in 2015 using multigap resistive plate chamber technology, providing a time resolution of 60 ps [16].

Simulated data samples produced with GEANT4-based [17] Monte Carlo (MC) software, which includes the geometric description of the BESIII detector and its response, are used to determine detection efficiencies and to estimate backgrounds. The simulation models the beam energy spread and initial state radiation in the e^+e^- annihilations with the generator KKMC [18]. The inclusive MC sample includes both the production of the J/ψ resonance and the continuum processes incorporated in KKMC. The known decay modes are modeled with EVTGEN [19] using branching fractions taken from the Particle Data Group (PDG) [8], and the remaining unknown charmonium decays are modeled with LUNDCHARM [20]. Final state radiation from charged final

state particles is incorporated using PHOTOS [21]. The decay $J/\psi \rightarrow \gamma\eta'$ is generated with an angular distribution of $1 + \cos^2_{\theta_\gamma}$, while the decay $\eta' \rightarrow e^+e^-e^+e^-$ is generated with a specific model based on the resonance chiral symmetric theory with SU(3) breaking [7].

III. DATA ANALYSIS

Four charged particles with zero net charge are required to be within the range of $|\cos \theta| < 0.93$, where θ is defined with respect to the z axis, which is the symmetry axis of the MDC. The distance of closest approach to the interaction point (IP) must be less than 10 cm along the z direction, and less than 1 cm in the plane transverse to the z axis. Particle identification (PID) for charged tracks combines measurements of the energy deposited in the MDC (dE/dx) and the flight time in the TOF to form likelihoods the electron [$\mathcal{L}(e)$], pion [$\mathcal{L}(\pi)$], and kaon [$\mathcal{L}(K)$] hypotheses. Tracks are identified as electrons when the the electron hypotheses satisfy $\mathcal{L}(e) > 0.001$ and has the highest PID likelihood among the three hypotheses, i.e. $\mathcal{L}(e) > \mathcal{L}(\pi)$ and $\mathcal{L}(e) > \mathcal{L}(K)$. To reduce background from hadrons and muons, the electron and positron candidates with higher momentum must satisfy $E/cp > 0.8$, where E is the deposited energy in the EMC and p is the momentum measured by the MDC [22–24].

Photon candidates are identified using showers in the EMC. The deposited energy of each shower must be more than 25 MeV in the barrel region ($|\cos \theta| < 0.80$) and more than 50 MeV in the end cap region ($0.86 < |\cos \theta| < 0.92$). To exclude showers that originate from charged tracks, the angle between the direction of each shower in the EMC and the direction of the closest extrapolated charged track must be greater than 10° . To suppress electronic noise and showers unrelated to the event, the difference between the EMC time and the event start time is required to be within $[0, 700]$ ns. At least one photon satisfying these selection criteria is required in the final state.

A vertex constraint on the four electrons is imposed to ensure they originate from the IP. To improve the resolution and suppress the background, a kinematic fit with an energy-momentum constraint (4C) is performed under the hypothesis of $J/\psi \rightarrow \gamma e^+e^-e^+e^-$. For a small portion of events with multiple photon candidates, all of them are looped in the 4C fit. According to the simulation study, the $\chi^2_{\gamma e^+e^-e^+e^-}$ distribution of the 4C fit could identify the correct photon candidate effectively, so only the combination with the smallest $\chi^2_{\gamma e^+e^-e^+e^-}$ is retained. The $\chi^2_{\gamma e^+e^-e^+e^-}$ distributions from data and signal MC are in a good agreement, as shown in Fig. 1. Events with $\chi^2_{\gamma e^+e^-e^+e^-} < 50$ are kept for further analysis. To suppress background events with $\gamma\pi^+\pi^-e^+e^-$ in the final state, a 4C kinematic fit is performed under the hypothesis of $J/\psi \rightarrow \gamma\pi^+\pi^-e^+e^-$, and $\chi^2_{\gamma e^+e^-e^+e^-}$ is required to be less than $\chi^2_{\gamma\pi^+\pi^-e^+e^-}$.

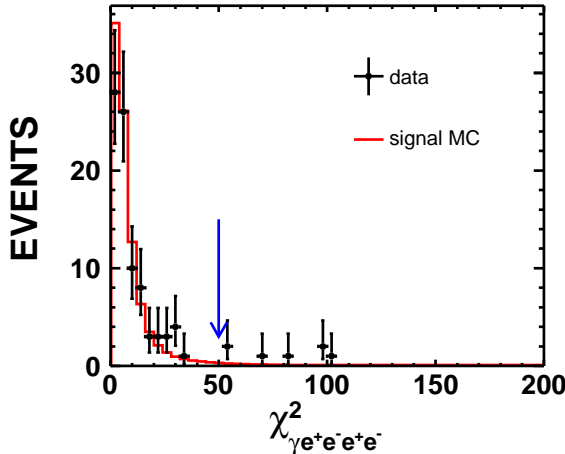


FIG. 1. The $\chi^2_{\gamma e^+e^-e^+e^-}$ distribution. The dots with error bars are from data, the red solid line is from signal MC. The arrow indicates the selection requirement of $\chi^2_{\gamma e^+e^-e^+e^-} < 50$.

The processes $J/\psi \rightarrow \gamma\eta'$ with $\eta' \rightarrow \gamma\gamma$, $\eta' \rightarrow \gamma e^+e^-$ and $\eta' \rightarrow \gamma\rho^0$, $\rho^0 \rightarrow e^+e^-$ may contribute peaking backgrounds to the invariant mass $M(e^+e^-e^+e^-)$ distributions, if the photons subsequently convert into e^+e^- pairs in the beam pipe or the inner wall of the MDC. To distinguish the γ conversion events from signal events, the Photon Conversion Finder package [25, 26] is used. Two variables are considered: (i) The distance $\delta_{xy} = \sqrt{R_x^2 + R_y^2}$ from the reconstructed vertices of the e^+e^- pairs to the IP in the transverse plane. Here, R_x and R_y represent the coordinates of the reconstructed vertex position in the x and y directions. The distributions of δ_{xy} for the data, γ conversion background, and signal from MC simulation are shown in Fig. 2. (ii) The angle θ_{eg} between the momentum vector of the radiative photon and the direction from IP to conversion point. In each event, there are four possible e^+e^- pairs. The event with any e^+e^- pair satisfying $\delta_{xy} \geq 2$ cm and $\cos \theta_{eg} \geq -0.50$ is rejected. This γ conversion veto requirement removes most of the γ conversion backgrounds with a relative detection efficiency loss less than 20%.

The signal region is defined as $0.9 < M(e^+e^-e^+e^-) < 1.0$ GeV/ c^2 . After applying the above selection criteria, the total detection efficiency is determined to be $(12.67 \pm 0.02)\%$ and the number of survived events is 86 as shown in Fig. 3.

The possible background contaminations are studied with an inclusive MC sample of 1.0011×10^{10} simulated events and data samples taken at $\sqrt{s} = 3.08$ and $\sqrt{s} = 3.773$ GeV. Since the cross section of $e^+e^- \rightarrow \gamma\eta'$ is less than 1 nb [7], the possible background from this process is negligible. For the dominant background channels, dedicated exclusive MC samples are generated to estimate their contributions. After applying all selection criteria, most backgrounds are negligible. The only remaining peaking background in the $e^+e^-e^+e^-$ mass spectrum

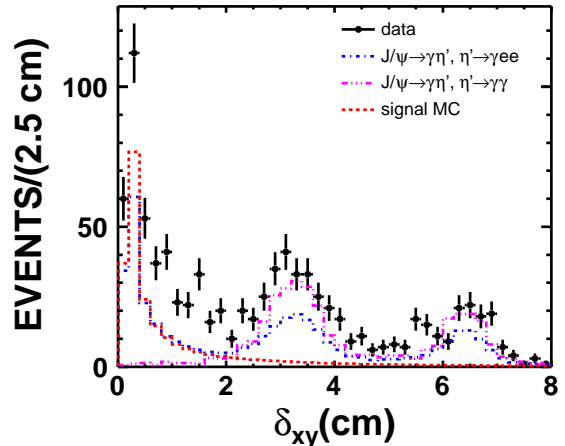


FIG. 2. The distribution of δ_{xy} . The black dots with error bars represent data, the red dashed histogram shows the signal MC simulation. The blue dash-dotted and magenta dash-dot-dotted histograms show the simulated γ conversion samples from $J/\psi \rightarrow \gamma\eta'$, $\eta' \rightarrow \gamma e^+e^-$ and $J/\psi \rightarrow \gamma\eta'$, $\eta' \rightarrow \gamma\gamma$, respectively.

comes from $J/\psi \rightarrow \gamma\eta'$, $\eta' \rightarrow \gamma e^+e^-$, with the number of expected events being 2.48 ± 0.18 after taking into consideration the BF from the PDG [8].

After the above selection, the resulting $M(e^+e^-e^+e^-)$ distribution is shown in Fig. 3, where a clear η' signal is visible. An unbinned extended maximum likelihood fit is performed to determine the η' signal yield. The signal probability density function (PDF) is represented by the signal MC shape convolved with a Gaussian function to account for the resolution difference between data and MC simulation. The shape for the nonpeaking background is described by a linear function. The background yield and its PDF parameters are allowed to float in the fit. The peaking background from the γ conversion process of $J/\psi \rightarrow \gamma\eta'$, $\eta' \rightarrow \gamma e^+e^-$ is described by the MC-simulated shape [27] with the yield fixed at 2.48.

The BF of $\eta' \rightarrow e^+e^-e^+e^-$ is calculated as

$$\mathcal{B}(\eta' \rightarrow e^+e^-e^+e^-) = \frac{N_{\text{signal}}}{N_{J/\psi} \cdot \mathcal{B}(J/\psi \rightarrow \gamma\eta') \cdot \epsilon} \quad (1) \\ = (4.5 \pm 1.0) \times 10^{-6},$$

where $N_{\text{signal}} = 30.1 \pm 7.0$ is the signal yield obtained from fitting, $N_{J/\psi}$ is the number of J/ψ events, ϵ is the MC-determined detection efficiency, and $\mathcal{B}(J/\psi \rightarrow \gamma\eta')$ is the BF of $J/\psi \rightarrow \gamma\eta'$ from the PDG [8]. The significance is determined by evaluating $\sqrt{-2\ln(\mathcal{L}_0/\mathcal{L}_{\max})}$, where $\mathcal{L}_0(\mathcal{L}_{\max})$ is the smeared likelihood without (with maximum) signal events. When the systematic uncertainties are taken into account by convolving the likelihood function of the signal yield with a Gaussian function, the significance is estimated to 5.7σ .

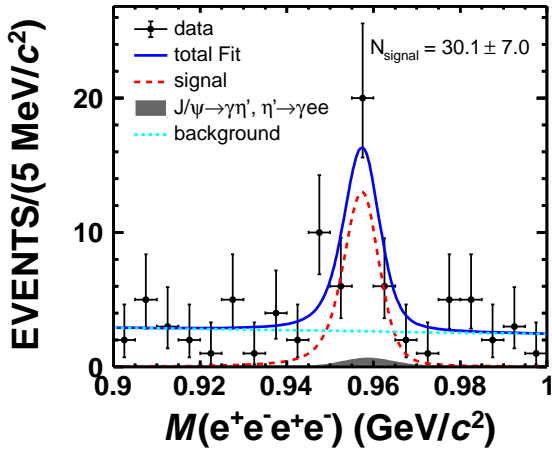


FIG. 3. The $M(e^+e^-e^+e^-)$ distribution of data and the fitting results. The dots with error bars are data, the red dashed line is the signal shape, and the solid blue line is the total fit result. The gray area represents the peaking background from $J/\psi \rightarrow \gamma\eta'$, $\eta' \rightarrow \gamma e^+e^-$, and the cyan dotted line is a linear function.

IV. SYSTEMATIC UNCERTAINTIES

Table I lists sources of systematic uncertainties considered in the BF measurement. Most systematic uncertainties are determined from comparisons of low-background, high-statistics data samples and MC simulation samples.

The PID and tracking efficiencies of electrons are determined from a control sample of radiative Bhabha scattering $e^+e^- \rightarrow \gamma e^+e^-$ (including $J/\psi \rightarrow \gamma e^+e^-$) corresponding to the center-of-mass energy of the J/ψ resonance. For the electron PID study, the same PID requirements as used in this analysis are applied to the control samples. Similarly, for the electron-tracking study, the same conditions on the polar angle and the distances of closest approach are used. Differences in PID (tracking) efficiencies between the data and MC simulations are obtained for each bin of a two-dimensional distribution of the momentum (transverse momentum) versus the polar angle of the electron tracks. These results are subsequently used to determine the overall weighted differences per track for PID and tracking, and the obtained PID and tracking uncertainties for electrons are 3.8% and 2.2%, respectively. The photon detection efficiency is studied with the control sample based on $J/\psi \rightarrow \pi^+\pi^-\pi^0$, $\pi^0 \rightarrow \gamma\gamma$ events [28]. The difference between data and MC simulation is 0.5% (1.5%) for a photon in the EMC barrel (end cap) region. Since most photon candidates are located in the barrel region, the difference 0.5% is taken as systematic uncertainty.

In the 4C kinematic fit, the track helix parameters are corrected to reduce the differences between data and MC simulation [27, 29]. The 2.7% difference between the efficiencies with and without helix parameter corrections is taken as the systematic uncertainty. The sys-

tematic uncertainty related with the γ conversion veto criterion has been investigated with a control sample of $e^+e^- \rightarrow \gamma e^+e^-$ at $\sqrt{s} = 3.08$ GeV, where the invariant mass of e^+e^- is limited to a range of extremely small mass (< 10 MeV/ c^2). The relative difference of efficiency associated with the γ conversion rejection criterion between data and MC simulation is 1.4%. Since the γ conversion veto criterion is used for two e^+e^- pairs in the final state, the total systematic uncertainty is 5.6%.

In the nominal signal MC model, the parameters describing $\eta - \eta'$ mixing and the $\pi^0 \rightarrow \gamma\gamma$ decay width are fixed. To estimate the systematic uncertainty due to the form-factor parametrizations, signal MC events are also generated using the global fit results from Ref. [7]. The relative difference 7.1% in the detection efficiency is taken as the uncertainty associated with the signal model.

The uncertainty due to the nonpeaking background shape is estimated by varying the PDF shape and fitting range. The fit range is changed to $(0.89, 1.01)$ or $(0.91, 0.99)$ GeV/ c^2 . A second-order Chebyshev polynomial is selected as an alternative background shape. A series of alternative fits are performed for all combinations of fit ranges and nonpeaking background shapes to account for possible correlations. The largest relative difference of the signal yield with respect to the nominal values, 2.7%, is taken as the systematic uncertainty. In the nominal fit, the number of peaking background events from $J/\psi \rightarrow \gamma\eta'$, $\eta' \rightarrow \gamma e^+e^-$ is fixed. To determine the systematic uncertainty, the number of peaking background events is varied within its uncertainty, and the resulting difference is negligible.

The uncertainty in the quoted BF of $J/\psi \rightarrow \gamma\eta'$ is 1.3% [8]. The uncertainty in the number of J/ψ events is determined to be 0.4% [12].

Assuming that all systematic uncertainties in Table I are independent, the total systematic uncertainty, obtained from their quadratic sum, is 10.8%.

TABLE I. The sources of systematic uncertainties and their estimated magnitudes. The negligible uncertainty is marked with an ellipsis.

Sources	Systematic uncertainties (in %)
PID	3.8
MDC tracking	2.2
Photon detection	0.5
4C kinematic fit	2.7
Veto of γ conversion	5.6
Signal model	7.1
Fit range and background shape	2.7
Peaking background	...
Quoted BF	1.3
Number of J/ψ	0.4
Total uncertainty	10.8

V. SUMMARY

Using a sample of about 1×10^{10} J/ψ events collected with the BESIII detector, we observe the double Dalitz decay process $\eta' \rightarrow e^+e^-e^+e^-$ via $J/\psi \rightarrow \gamma\eta'$, with a significance of 5.7σ after taking the systematic uncertainty into consideration. The BF of $\eta' \rightarrow e^+e^-e^+e^-$ is measured to be $(4.5 \pm 1.0(\text{stat.}) \pm 0.5(\text{sys.})) \times 10^{-6}$. The measured BF is consistent with the theoretical predictions within the uncertainties and provides new information for the studies about η' TFF and the interactions between η' and virtual photons [1, 2].

ACKNOWLEDGMENTS

The BESIII collaboration thanks the staff of BEPCII and the IHEP computing center for their strong support. We thank Feng Xu for useful discussions. This work is supported in part by National Key R&D Program of China under Contracts Nos. 2020YFA0406400, 2020YFA0406300; National Natural Science Foundation of China (NSFC) under Contracts Nos. 11625523, 11635010, 11735014, 11822506, 11835012, 11935015,

11935016, 11935018, 11961141012, 12022510, 12025502, 12035009, 12035013, 12061131003, 12165022; the Chinese Academy of Sciences (CAS) Large-Scale Scientific Facility Program; Joint Large-Scale Scientific Facility Funds of the NSFC and CAS under Contracts Nos. U1732263, U1832207; CAS Key Research Program of Frontier Sciences under Contract No. QYZDJ-SSW-SLH040; 100 Talents Program of CAS; INPAC and Shanghai Key Laboratory for Particle Physics and Cosmology; ERC under Contract No. 758462; European Union Horizon 2020 research and innovation programme under Contract No. Marie Skłodowska-Curie grant agreement No 894790; German Research Foundation DFG under Contracts Nos. 443159800, Collaborative Research Center CRC 1044, FOR 2359, GRK 214; Istituto Nazionale di Fisica Nucleare, Italy; Ministry of Development of Turkey under Contract No. DPT2006K-120470; National Science and Technology fund; Olle Engkvist Foundation under Contract No. 200-0605; STFC (United Kingdom); The Knut and Alice Wallenberg Foundation (Sweden) under Contract No. 2016.0157; The Royal Society, UK under Contracts Nos. DH140054, DH160214; The Swedish Research Council; U. S. Department of Energy under Contracts Nos. DE-FG02-05ER41374, DE-SC-0012069.

-
- [1] R. Escribano *et al.*, Chin. Phys. C **42**, 023109 (2018).
 - [2] T. Petri, arXiv: 1010.2378[nucl-th].
 - [3] T. Aoyama *et al.*, Phys. Rep. **887**, 1 (2020).
 - [4] A. Keshavarzi *et al.*, Phys. Rev. D **97**, 114025 (2018).
 - [5] R. Escribano *et al.*, Phys. Rev. D **89**, 034014 (2014).
 - [6] Johan Bijnens *et al.*, arXiv: hep-ph/0106130v1.
 - [7] H. Czyż *et al.*, Phys. Rev. D **97**, 016006 (2018).
 - [8] P.A. Zyla *et al.* (Particle Data Group), Prog. Theor. Exp. Phys. **2020**, 083C01 (2020).
 - [9] E. Abouzaid *et al.* (KTeV Collaboration), Phys. Rev. Lett. **100**, 182001 (2008).
 - [10] F. Ambrosino *et al.* (KLOE Collaboration), Phys. Lett. B **702**, 324 (2011).
 - [11] M. Berlowski *et al.* (CELSIUS/WASA Collaboration), Phys. Rev. D **77**, 032004 (2008).
 - [12] M. Ablikim *et al.* (BESIII Collaboration), arXiv: 2111.07571.
 - [13] M. Ablikim *et al.* (BESIII Collaboration), Nucl. Instrum. Meth. A **614**, 345 (2010).
 - [14] C. H. Yu *et al.*, Proceedings of IPAC2016, Busan, Korea (JACoW, Geneva, Switzerland, 2016), <https://doi.org/10.18429/JACoW-IPAC2016-TUYA01>.
 - [15] M. Ablikim *et al.* (BESIII Collaboration), Chin. Phys. C **44**, 040001 (2020).
 - [16] X. Li *et al.*, Radiat. Detect. Technol. Methods **1**, 13 (2017); Y. X. Guo *et al.*, Radiat. Detect. Technol. Methods **1**, 15 (2017); P. Cao *et al.*, Nucl. Instrum. Meth. A **953**, 163053 (2020).
 - [17] S. Agostinelli *et al.* (GEANT4 Collaboration), Nucl. Instrum. Meth. A **506**, 250 (2003).
 - [18] S. Jadach, B. F. L. Ward and Z. Was, Phys. Rev. D **63**, 113009 (2001); Comput. Phys. Commun. **130**, 260 (2000).
 - [19] D. J. Lange, Nucl. Instrum. Meth. A **462**, 152 (2001); R. G. Ping, Chin. Phys. C **32**, 599 (2008).
 - [20] J. C. Chen, G. S. Huang, X. R. Qi, D. H. Zhang, and Y. S. Zhu, Phys. Rev. D **62**, 034003 (2000); R. L. Yang, R. G. Ping, and H. Chen, Chin. Phys. Lett. **31**, 061301 (2014).
 - [21] E. Richter-Was, Phys. Lett. B **303**, 163 (1993).
 - [22] M. Ablikim *et al.* (BESIII Collaboration), Phys. Rev. D **96**, 111101 (2017).
 - [23] M. Ablikim *et al.* (BESIII Collaboration), Phys. Lett. B **783**, 452 (2018).
 - [24] M. Ablikim *et al.* (BESIII Collaboration), Phys. Rev. D **103**, 112007 (2021).
 - [25] Z. R. Xu and K. L. He, Chin. Phys. C **36**, 742 (2012).
 - [26] M. Ablikim *et al.* (BESIII Collaboration), Phys. Rev. D **104**, 092004 (2021).
 - [27] M. Ablikim *et al.* (BESIII Collaboration), Phys. Rev. D **92**, 012001 (2015).
 - [28] M. Ablikim *et al.* (BESIII Collaboration), Phys. Rev. D **83**, 112005 (2011).
 - [29] M. Ablikim *et al.* (BESIII Collaboration), Phys. Rev. D **87**, 012002 (2013).